MATERIALS SCIENCE

Artificial 3D hierarchical and isotropic porous polymeric materials

Stefan Chisca,[1] Valentina-Elena Musteata,[1] Rachid Sougrat,[2] Ali Reza Behzad,[2] Suzana P. Nunes[1]*

Hierarchical porous materials that replicate complex living structures are attractive for a wide variety of applications, ranging from storage and catalysis to biological and artificial systems. However, the preparation of structures with a high level of complexity and long-range order at the mesoscale and microscale is challenging. We report a simple, nonextractive, and nonreactive method used to prepare three-dimensional porous materials that mimic biological systems such as marine skeletons and honeycombs. This method exploits the concurrent occurrence of the self-assembly of block copolymers in solution and macrophase separation by nucleation and growth. We obtained a long-range order of micrometer-sized compartments. These compartments are interconnected by ordered cylindrical nanochannels. The new approach is demonstrated using polystyrene-*b*-poly(*t*-butyl acrylate), which can be further explored for a broad range of applications, such as air purification filters for viruses and pollution particle removal or growth of bioinspired materials for bone regeneration.

INTRODUCTION

Shapes and patterns in nature have always fascinated scientists. For example, the symmetrical structure of radiolaria mineral skeletons, the perfect hexagonal order of bee honeycombs, or cellular clusters forming a fly's eye are governed by mechanisms that minimize surface energy and area. Inspired by these patterns, scientists have created artificial hierarchical porous materials that have a well-balanced surface area, mechanical stability, and the ability for selective transport. As such, they can be used in biomedical applications, separation, and catalytic processes (*1*–*5*). However, replicating nature's complex three-dimensional (3D) geometries at the nanoscale to yield materials with a long-range order is challenging and difficult to achieve.

Self-assembly of block copolymers is one of a few approaches that have been used to prepare these hierarchical systems (*6*–*8*). One of the reasons for using these polymers is their equilibrium morphologies in the form of spheres, cylinders, bicontinuous gyroids, and lamellae (*9*–*13*). Their assembly in solution leads to an even richer variety of structures (for example, disk-sphere, disk-cylinder, rectangular platelets, or quasicrystalline) (*14*–*17*). For example, hierarchical nanoporous particles and 3D films could be obtained by the addition of soluble additives during film formation (*18*, *19*) or by thermal CO_2 laser-induced patterned polymerization (*20*). The porous structure is most commonly produced by the selective extraction of soluble components. However, the generation of porous materials without etching or an extraction step has been much more restricted. A good example is the formation of spherical particles (1D structures, micrometer-sized) with highly ordered nanopores in a confined space (*21*), which resemble Schwarz's bicontinuous periodic minimal surfaces. A more frequently explored example is the preparation of 2D porous asymmetric architectures with regular hexagonally ordered pores (*22*–*24*) by self-assembly in solution and immersion in water. These 2D films mainly consisted of a thin (<400 nm) ordered layer on top of a disordered substructure. Expanding the structures from 2D to 3D could significantly broaden the possibilities for application. For instance, it is known that the biological activity of cells is much higher if the cells are grown on 3D scaffolds (*25*). To date, the use of polyHIPES (porous emulsion-templated porous polymers synthesized within high internal phase emulsions) has been an effective alternative method for one-pot preparation of monoliths with hierarchically isotropic pores with a diameter in the micrometer scale (*26*). Analogous structures at the nanometer scale were only reported on the basis of breath figures (*27*), applied to the amphiphilic polystyrene-*b*-poly(*N*,*N*-dimethylacrylamide) copolymer. This method, however, requires a severe control of humidity and uses nonpolar solvents.

We propose here a simple method to obtain flexible films with complex hierarchical and isotropic porous structures within 5 min. We demonstrate this method using polystyrene-*b*-poly(*tert*-butyl acrylate) (PS-*b*-PtBA). These films are constituted by micrometer-sized compartments, which are interconnected by long-range hexagonally ordered nanochannels (Fig. 1, A and B).

RESULTS AND DISCUSSION

We prepared porous structures by using 20 weight % (wt %) of PS_{636}-*b*-$PtBA_{250}$ (subscripts refer to the number-average degree of polymerization) solutions in *N*,*N*′-dimethylformamide (DMF) mixtures with tetrahydrofuran (THF) or 1,4-dioxane (DOX). The solvent weight ratio was kept as 1:3 THF (or DOX)/DMF, and the resulting solution was cast on a glass plate and evaporated for 10 s to 10 min at room temperature. The Flory-Huggins parameters (χ) for these systems ($\chi_{DMF\text{-}PS}$ = 1.25 and $\chi_{DMF\text{-}PtBA}$ = 1.6, $\chi_{THF\text{-}PS}$ = 0.32 and $\chi_{THF\text{-}PtBA}$ = 0.31, and $\chi_{DOX\text{-}PS}$ = 0.42 and $\chi_{DOX\text{-}PtBA}$ = 0.38) indicated that DMF was a poor solvent for the PS-*b*-PtBA copolymer, in the limit of thermodynamic stability, whereas THF and DOX were better solvents. The solution layer became turbid after 10 s of evaporation. This indicates that a macrophase separation initiates, with no further visual change observed after 5 min. The film was then immersed in water to extract the remaining solvent and to interrupt the phase separation after short evaporation times (*28*).

As shown by scanning electron microscopy (SEM) images (Fig. 1C and fig. S1), at the macroscale, spherical capsules of increasing size are formed as the evaporation time increases from 10 to 30 s, whereas at the mesoscale, hexagonal cylinders are simultaneously generated (Fig. 2, B to D). Taking into account the regularly spherical morphology of the capsules, we hypothesized that the phase separation follows the nucleation and growth (NG) mechanism. Then, we investigated how an additive, such as β-cyclodextrin (β-CD), influences the formation of a

[1]Biological and Environmental Science and Engineering Division, King Abdullah University of Science and Technology, Thuwal 23955-6900, Saudi Arabia. [2]Advanced Nanofabrication Imaging and Characterization Laboratory, King Abdullah University of Science and Technology, Thuwal, 23955-6900, Saudi Arabia.
*Corresponding author. Email: suzana.nunes@kaust.edu.sa

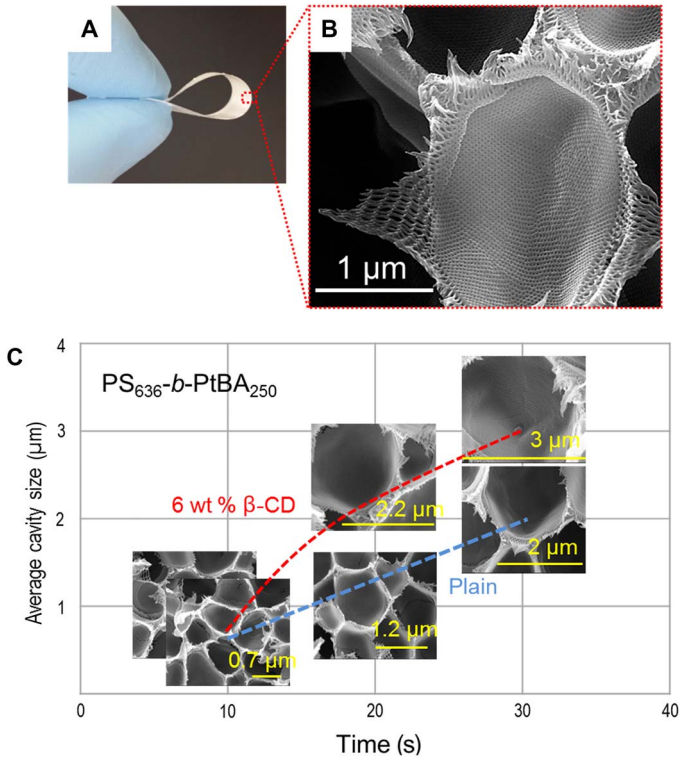

Fig. 1. Self-assembly of PS_{636}-*b*-$PtBA_{250}$ into a hierarchical structure. (**A**) Optical image of a PS_{636}-*b*-$PtBA_{250}$ film cast from 20 wt % solution in 1:3 (wt %) THF/DMF on a glass plate. (**B**) Corresponding SEM cross-sectional image after 5 min of evaporation with details of a macrocavity and its fine mesoporous structure. (**C**) Plot of the average cavity diameter, measured by SEM, as a function of evaporation time (10, 20, and 30 s); effect of the addition of 6 wt % β-CD (calculated with respect to block copolymer amount) to the casting solution.

hierarchical structure when it interacts with *t*-butyl acrylate segments (*29*). β-CD accelerated the NG kinetics, the nuclei growth, and, as a consequence, the increase of block copolymer concentration in the matrix (Fig. 1C and fig. S1). By increasing the evaporation time from 30 s to 1 and 5 min, we achieved a better long-range hexagonal order in bulk and at the surface (fig. S2).

Full reconstruction (macroscale and mesoscale) of the 3D images enabled a better overview of the hierarchical structure. We combined two complementary advanced microscopy techniques: (i) serial block face SEM (Fig. 2A) to image the macrostructure and overview the scaffold architecture and (ii) transmission electron microscopy (TEM) tomography (Fig. 2D) to image the fine mesoscale structure so that details of the walls between the spherical compartments can be shown. The spherical compartments measured up to 5 μm in diameter (Fig. 2A). These compartments were highly interconnected, as shown by TEM tomography (Fig. 2D). Ruthenium tetroxide (RuO_4) staining of the TEM image shows nanochannels connecting the compartments (Fig. 2C).

To gain insight into the mesoscale order formation in solution, we performed small-angle x-ray scattering (SAXS). The order of PS_{636}-*b*-$PtBA_{250}$ solutions in THF/DMF improved as the polymer concentration increased or when β-CD was added (Fig. 3, A and B). The intensity of the primary peak (q^*) increased and slightly shifted to lower q for both conditions (with or without β-CD) as the concentration changed from 20 to 35 wt %. The broad scattering shoulder transformed into a sharp primary peak when the concentration increased to 42 wt % for plain solutions (Fig. 3A). In contrast, a sharp primary peak for solutions with β-CD already appeared at the 37 wt % block copolymer (Fig. 3B). This indicates that the β-CD facilitates the self-assembly process. Furthermore, the patterns characteristic to the hexagonal lattice ($q/q^* = 1, \sqrt{3}, 2, \sqrt{7}, 3$, and $\sqrt{12}$) could be seen at 42 wt % in the presence of β-CD, while for the plain solutions, it could be seen at 45 wt %. These SAXS patterns for different concentrations reflect the changes in

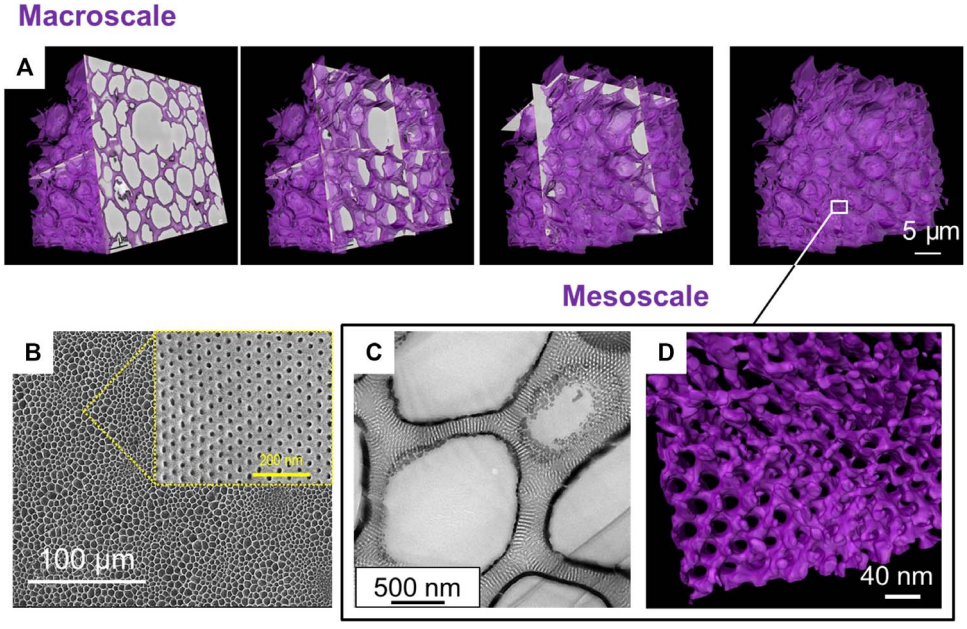

Fig. 2. Macroscale and mesoscale long-range order of hierarchical structures obtained from PS_{636}-*b*-$PtBA_{250}$ solutions in 1:3 (wt %) DOX/DMF after 5 min of evaporation. (**A**) Three-dimensional reconstruction of SEM images by serial block face. (**B**) SEM surface. (**C**) Cross-sectional TEM image stained with RuO_4; (**D**) TEM tomography: 3D surface rendering of a thin section of the film.

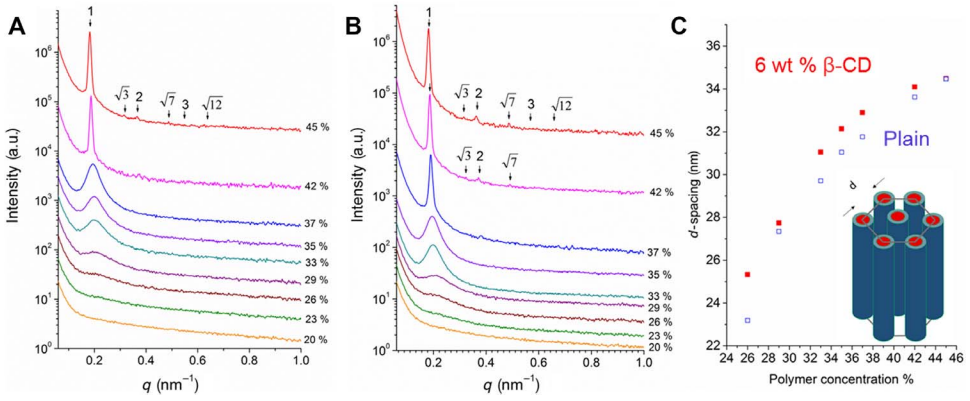

Fig. 3. SAXS characterization of the mesoscale order of PS_{636}-*b*-$PtBA_{250}$ in solutions with different copolymer concentrations (wt %) in 1:3 (wt %) THF/DMF. (**A**) Plain solutions and (**B**) solutions with 6 wt % β-CD. (**C**) Periodic distance in solution as a function of copolymer concentration. a.u., arbitrary units.

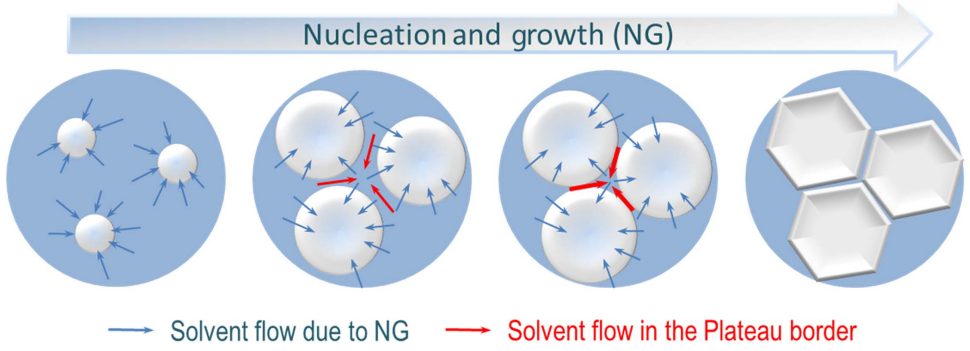

Fig. 4. Macroscale structure formation. Scheme of NG development: Nuclei growth and simultaneous solvent flow from the polymer-rich matrix to the polymer-depleted nuclei (blue arrows); solvent flow in the Plateau border between nuclei (red arrows).

morphology observed by SEM, as evaporation time increases. From the position of the first peak, the periodic distances between ordered domains were estimated as a function of concentration (Fig. 3C).

Similar behavior was observed when using THF or DOX in the solvent mixtures, but the better long-range order was obtained with DOX. In particular, the order on the surface is improved with DOX (Fig. 2B), and the effect of β-CD becomes less evident (fig. S3). We observed a honeycomb architecture similar to that created by nature at the macroscale and mesoscale (fig. S3D). The mesoscale pore sizes and their distributions at the surface and in bulk are similar (pore diameter, 15 ± 1 nm; fig. S5), indicating that our approach can precisely control the morphology at the mesoscale range. SAXS investigation confirmed that the mesoscale (*p6mm*) hexagonal order appears at higher evaporation time (fig. S4, A and B).

We believe that the 3D hierarchical structure is formed by the co-occurrence of a macrophase separation following the NG mechanism (Fig. 4) and the block copolymer self-assembly. The systems we present here are on the verge of thermodynamic instability with high block-solvent Flory-Huggins interaction parameters (table S1) (*30*). The Flory-Huggins interaction parameter depends on polymer concentration (*31*), and it might even deteriorate as the solvent evaporates. NG is promoted when the system is kept for some time under a thermodynamically metastable condition, which could be, in this case, induced when the solvent is partially evaporated, and the concentration of the copolymer simultaneously increases. In our investigated system, the nucleating phase is depleted of polymer and grows as time evolves. If a typical mechanism of NG is at work, the nuclei composition remains constant while their radius increases. When the polymer-depleted spherical nuclei continue to grow and come together, they flatten at the intersection if their size is practically equal. Nuclei of different sizes might tend to coalesce because different curvatures would lead to different internal pressures according to Young-Laplace. In analogy to what happens in surfactant foams, hexagonal or heptagonal cells of similar size, separated by thin walls, are formed. As NG proceeds, the solution mass transfer inside these walls is directed to the intersection between three nuclei, the Plateau border (red arrows in Fig. 4) (*32*). At the same time, solvent transfer continues to occur from the already polymer-concentrated phase to the depleted nuclei. This flow (blue arrows in Fig. 4) promotes the self-assembly of the block copolymer confined in the thin walls. As a result, channels connecting the adjacent spherical compartments are formed. As more solvent leaves the wall, the mobility of the polymer system decreases, and the system gels. To exclude the contribution of the breath figures' mechanism in the formation of the structure, we prepared porous films at different, relative humidity levels. Similar morphology was obtained at humidity higher than 60% and lower than 20% (fig. S6), in contrast to what is normally reported for breath figures, which are preferentially formed at higher humidity (80%). In addition, breath figures are favored in the presence of nonpolar solvents and not in the presence of highly polar solvents such as DMF, which we used for this method (*33*). Breath figures mostly lead to regular porosity only on the upper layers of films. Our system yields an order in isotropic films as thick as 50 μm. We have shown that this new approach could be

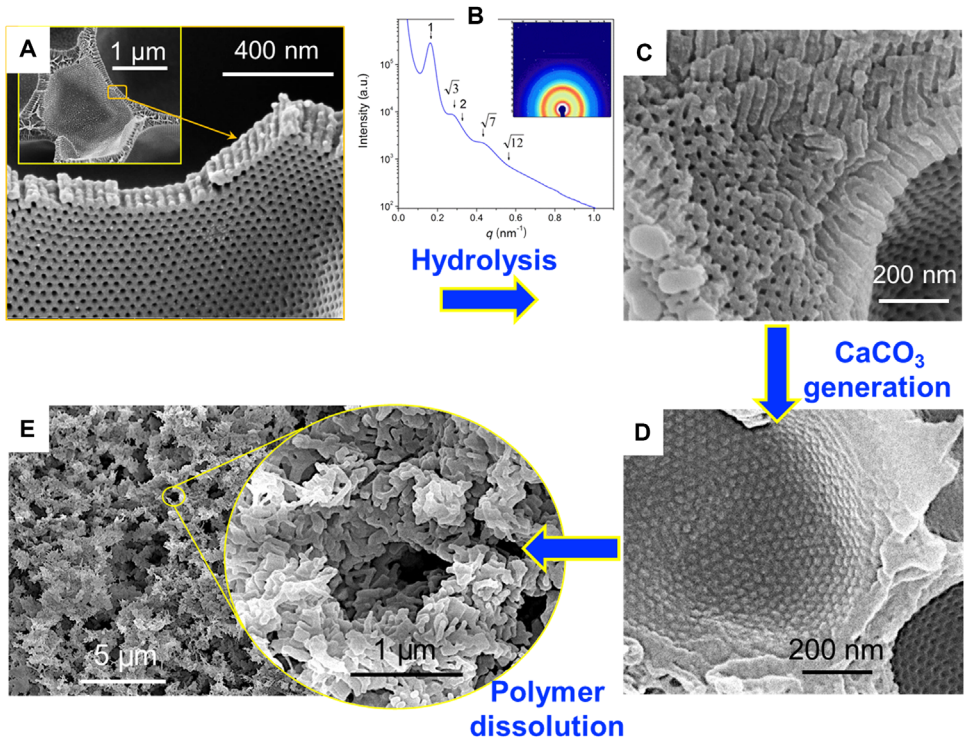

Fig. 5. $CaCO_3$ mineralization in block copolymer scaffolds. (**A**) SEM images of scaffolds obtained from PS_{636}-*b*-$PtBA_{250}$ solutions in 1:3 (wt %) DOX/DMF after 5 min of evaporation. (**B**) SAXS and (**C**) SEM of the scaffold after hydrolysis with TFA for 24 hours. (**D**) Scaffolds filled with $CaCO_3$ generated by the reaction between $CaCl_2$ and $(NH_4)_2CO_3$. (**E**) Remaining inorganic structure after polymer dissolution.

extended to different PS-*b*-PtBA molecular weights (fig. S7), and we expect to obtain similar structures with other copolymer systems close to a metastable condition.

The morphology and porosity scale of these films are very convenient for air purification filters, which target the elimination of viruses, such as echovirus or rhinovirus, or pollution particles with a size in the range of 20 to 30 nm (*34*). Particles of this size should be removed by the mesoporous structure, as shown in Fig. 5A. Because these pores cover the walls of all compartments, which are distributed in the whole film, the particles can repeatedly be excluded with high efficiency when flowing through the porous structure. On the other hand, the large compartments make the films less dense and decrease the resistance to air flow. The air flow of a 50-μm isotropic PS_{636}-*b*-$PtBA_{250}$ film is 0.12 $m^3\ m^{-2}\ hour^{-1}\ bar^{-1}$.

Moreover, we converted the PtBA block to poly(acrylic acid) (PAA) (Fig. 5 and fig. S8), making this system a starting platform for other applications, such as adsorption and removal of heavy metals (*35*, *36*), which require hydrophilic materials or further functionalization. Because of the presence of carboxylic groups and the unique morphology, a targeted application could be to use the now converted PS-*b*-PAA isotropic film as a scaffold to grow porous inorganic materials (*37*). As a proof of concept, we grew porous calcium carbonate ($CaCO_3$), which is known as a bioinspired material for bone regeneration (*38*). Figure 5C shows the SEM images for the PS-*b*-PAA, which demonstrates that after hydrolysis of the PtBA block, the 3D hierarchical structure is maintained. Moreover, the characteristic hexagonal order was confirmed by SAXS in Fig. 5B ($q/q^* = 1, \sqrt{3}, 2, \sqrt{7}$, and $\sqrt{12}$). Figure 5D shows the SEM images of the scaffold filled with $CaCO_3$. After the copolymer dissolution, a very porous $CaCO_3$ skeleton is left (Fig. 5E). This morphology indicates that the crystal's growth takes place in the hexagonal mesopores. The PAA blocks facilitate the transport of the calcium ions for the $CaCO_3$ formation (*39*).

In conclusion, we propose a new and versatile method to obtain well-defined 3D hierarchical structures that have tunable compartments and interconnected hexagonally ordered nanochannels at the macroscale and mesoscale. These structures are formed by solution NG and block copolymer self-assembly. This method allows us to rapidly achieve a long-range order, which can be tuned by changing the solvent and the block molecular weight or by adding β-CD. We anticipate that this class of materials could be used for storage, catalysis, transport, and drug delivery, and as air purification filters and scaffolds to design bioinspired materials.

MATERIALS AND METHODS

Materials

PS-*b*-PtBA copolymers with different degrees of polymerization [PS_{636}-*b*-$PtBA_{250}$ and PS_{677}-*b*-$PtBA_{180}$ (subscripts refer to the number-average degree of polymerization)] were purchased from Polymer Source Inc. The polydispersity values were 1.05 and 1.10, respectively. THF, DOX, DMF, and β-CD were purchased from Sigma-Aldrich. Dehydrated calcium chloride ($CaCl_2$) and ammonium carbonate [$(NH_4)_2CO_3$)] were purchased from Acros Organics. Trifluoroacetic acid (TFA) was purchased from Fisher Scientific. All chemicals were used as received.

Synthesis

Synthesis of isotropic films with a 3D hierarchical structure

In a typical procedure, 50 mg of PS_{636}-*b*-$PtBA_{250}$ was dissolved in 200 mg of solvent mixture (THF/DMF or DOX/DMF) to obtain 20%

concentration of the block copolymer. The ratio between the solvents in the mixture was kept constant at 1:3 THF/DMF or DOX/DMF. The obtained solution was cast on a glass plate using a casting knife with a 200-μm gap and was then evaporated from 10 s to 10 min. After 10 s of evaporation, the cast solution started to become turbid. After 5 min, no visual change was observed. To quench the phase separation after short evaporation times or to extract the remaining solvent, the system was immersed in water. When β-CD was used as an additive, a similar procedure was followed. The amount of β-CD was 6% with respect to the block copolymer, and the ratio between PS-*b*-PtBA and the solvent mixture was maintained at 20%. A similar procedure was used to obtain films from PS_{677}-*b*-$PtBA_{180}$.

Synthesis of isotropic PS-b-PAA films with a 3D hierarchical structure

The PS_{636}-*b*-$PtBA_{250}$ film was immersed into TFA solution and was gently stirred at room temperature for 24 hours (*37*). Afterward, the film was washed five times with water. To prove that the hydrolysis took place, we performed nuclear magnetic resonance (NMR) spectroscopy and Fourier transform infrared (FTIR) spectroscopy (fig. S8, A and B).

Synthesis of porous $CaCO_3$ using PS-b-PAA films with a 3D hierarchical structure

Porous $CaCO_3$ was obtained by immersing the PS-b-PAA films into a vial containing 50 mM $CaCl_2$ dissolved in a mixture of water/methanol (80:20) solution. After the system was degassed under vacuum for 12 hours, the vials were covered with needle-punctured parafilm (<5 needle holes) and placed in a closed desiccator that contains a needle-punctured vial (<5 needle holes) with $(NH_4)_2CO_3$ (*39*). The system was allowed to react for 5 days to obtain porous $CaCO_3$. Afterward, the template was removed by washing gently with water and ethanol for 24 hours. The template was removed by washing with DMF for 24 hours and THF for 6 hours, followed by washing with ethanol.

Characterization

The morphology of the 3D hierarchical structures was investigated by SEM via Nova Nano and Magellan microscopes using an accelerating voltage of 2 to 5 kV and a working distance of 1.5 to 5 mm. The samples were coated before measurement with iridium or with platinum using a Quorum Q150TES equipment. The samples for cross section were stained with RuO_4 before they were fractured in liquid nitrogen. The bulk morphology was also studied by TEM. Initially, the films were embedded in epoxy resin and cured at 60°C, and then ultrathin sections (70 nm) were cut using an ultramicrotome (Leica EM UC6). The films were stained with RuO_4 before imaging them with a Titan CT (FEI Company) microscope operating at 300 kV.

The 3D reconstruction of the macroscale structure was carried out using serial block face SEM. Small pieces of Ru-red–stained films were embedded in epoxy resin for serial block face cross-sectional imaging. Serial block face sectioning (at 50- or 100-nm imaging intervals) and imaging were performed using a Gatan 3View system (Gatan) mounted in an FEI Quanta FEG 200 microscope (FEI Company). The microscope was operated at an accelerating voltage of 2.0 kV and at a pressure of 30 Pa in low vacuum mode. A solid-state backscatter detector was used to acquire serial section images (stacks of 800, 632, and 500 sections) from three regions of interest. Three-dimensional segmentation and reconstruction of the film were performed using Avizo Fire 8.0 software. In addition, we performed the 3D reconstruction of the mesoscale structure by using TEM tomography. Titan CT (FEI Company) was used to perform the TEM tomography. The system operated at 300 kV and was equipped with a 4k × 4k charge-coupled device camera (Gatan). Xplore 3D tomography software (FEI Company) was used to acquire the tilt series for tomographic reconstruction. The sample was tilted from −65° to +65°, and images were captured at 2° initial intervals following a Saxton scheme. The tomograms were generated using a back projection algorithm as implemented in the IMOD software. Three-dimensional segmentation and reconstruction of the film were performed using Avizo Fire 8.0 software. To count the pores and to estimate the average pore size, we used the ImageJ software.

SAXS measurements for the block copolymer films and solutions were performed at the SAXS1 beamline of the Brazilian Synchrotron facility [Laboratorio Nacional de Luz Sincrotron (LNLS)], which worked at an energy of 8.0 keV. The x-ray wavelength was 0.155 nm, the distance from the sample to the detector was 3.057 m, and the beam area on the sample was 1 mm^2. The exposure time was 600 s, and the 2D scattering patterns were recorded by a PILATUS 300K detector with a pixel size of 172 μm × 172 μm. Plots of intensity versus scattering vector (q) were obtained by the radially integrated 2D patterns after normalization to the intensity of the primary beam and subtraction of the background. The position of the scattering peaks was obtained by fitting the data with a sum of Lorentz functions using Igor Pro 6.37 software (*40*).

The hydrolyzing of the PtBA block to PAA was proved by NMR spectroscopy. The sample was dissolved in DMF-d7, and the spectrum was recorded on a Bruker Avance III 400 spectrometer. Moreover, the conversion of the PtBA block into the PAA block was confirmed by FTIR spectroscopy. The FTIR spectrum was recorded by performing 16 scans with a spectral resolution of 4 cm^{-1}, at room temperature, on a Nicolet 6700 FT-IR System with a continuum infrared microscope.

Air permeance was measured using a constant volume/variable pressure method. The effective area of the film was approximately 2.8 cm^2. The experiments were performed at 25°C and 1 bar.

SUPPLEMENTARY MATERIALS

Supplementary material for this article is available at http://advances.sciencemag.org/cgi/content/full/4/5/eaat0713/DC1

Supplementary text on Flory-Huggins parameter estimation

table S1. Flory-Huggins interaction parameters (χ) between copolymer blocks and the solvent mixture.

fig. S1. Hierarchical structure of PS_{636}-*b*-$PtBA_{250}$ films obtained after evaporation times varying from 10 to 30 s, before immersion in the nonsolvent bath.

fig. S2. Hierarchical structure of PS_{636}-*b*-$PtBA_{250}$ films after long evaporation times.

fig. S3. Influence of the addition of β-CD to the PS_{636}-*b*-$PtBA_{250}$/DOX/DMF system on the macroscale.

fig. S4. Influence of the addition of β-CD to the PS_{636}-*b*-$PtBA_{250}$/DOX/DMF system on the mesoscale.

fig. S5. Mesopore dimensions of PS_{636}-*b*-$PtBA_{250}$ films prepared from solutions in 1:3 (wt %) DOX/DMF.

fig. S6. Effect of the relative humidity on the cross-section morphology of PS_{636}-*b*-$PtBA_{250}$ films obtained from solutions in 1:3 (wt %) DOX/DMF, after 5-min evaporation.

fig. S7. Hierarchical structure prepared from PS_{677}-*b*-$PtBA_{180}$ dissolved in 1:3 (wt %) DOX/DMF.

fig. S8. Hydrolysis of preformed hierarchical PS_{636}-*b*-$PtBA_{250}$ films to PS-*b*-PAA.

REFERENCES AND NOTES

1. G. M. Whitesides, B. Grzybowski, Self-assembly at all scales. *Science* **295**, 2418–2421 (2002).
2. A. H. Gröschel, A. H. E. Müller, Self-assembly concepts for multicompartment nanostructures. *Nanoscale* **7**, 11841–11876 (2015).
3. D. J. Lunn, J. R. Finnegan, I. Manners, Self-assembly of "patchy" nanoparticles: A versatile approach to functional hierarchical materials. *Chem. Sci.* **6**, 3663–3673 (2015).
4. T. P. J. Knowles, T. W. Oppenheim, A. K. Buell, D. Y. Chirgadze, M. E. Welland, Nanostructured films from hierarchical self-assembly of amyloidogenic proteins. *Nat. Nanotechnol.* **5**, 204–207 (2010).

5. X.-Y. Yang, L.-H. Chen, Y. Li, J. C. Rooke, C. Sanchez, B.-L. Su, Hierarchically porous materials: Synthesis strategies and structure design. *Chem. Soc. Rev.* **46**, 481–558 (2017).
6. S. C. Glotzer, M. J. Solomon, Anisotropy of building blocks and their assembly into complex structures. *Nat. Mater.* **6**, 557–562 (2007).
7. T. Aida, E. W. Meijer, S. I. Stupp, Functional supramolecular polymers. *Science* **335**, 813–817 (2012).
8. A. H. Gröschel, A. Walther, T. I. Löbling, F. H. Schacher, H. Schmalz, A. H. E. Müller, Guided hierarchical co-assembly of soft patchy nanoparticles. *Nature* **503**, 247–251 (2013).
9. F. S. Bates, G. H. Fredrickson, Block copolymers–designer soft materials. *Phys. Today* **52**, 32–38 (1999).
10. F. S. Bates, M. A. Hillmyer, T. P. Lodge, C. M. Bates, K. T. Delaney, G. H. Fredrickson, Multiblock polymers: Panacea or Pandora's box? *Science* **336**, 434–440 (2012).
11. Y. Mai, A. Eisenberg, Self-assembly of block copolymers. *Chem. Soc. Rev.* **41**, 5969–5985 (2012).
12. J-F. Lutz, J.-M. Lehn, E. W. Meijer, K. Matyjaszewski, From precision polymers to complex materials and systems. *Nat. Rev. Mat.* **1**, 16024 (2016).
13. S. P. Nunes, Block copolymer membranes for aqueous solution applications. *Macromolecules* **49**, 2905–2916 (2016).
14. H. Cui, Z. Chen, S. Zhong, K. L. Wooley, D. J. Pochan, Block copolymer assembly via kinetic control. *Science* **317**, 647–650 (2007).
15. J. Zhu, S. Zhang, K. Zhang, X. Wang, J. W. Mays, K. L. Wooley, D. J. Pochan, Disk-cylinder and disk-sphere nanoparticles via a block copolymer blend solution construction. *Nat. Commun.* **4**, 2297 (2013).
16. S. Lee, M. J. Bluemle, F. S. Bates, Discovery of a Frank-Kasper σ phase in sphere-forming block copolymer melts. *Science* **330**, 349–353 (2010).
17. H. Qiu, Y. Gao, C. E. Boott, O. E. C. Gould, R. L. Harniman, M. J. Miles, S. E. D. Webb, M. A. Winnik, I. Manners, Uniform patchy and hollow rectangular platelet micelles from crystallizable polymer blends. *Science* **352**, 697–701 (2016).
18. M. Seo, M. A. Hillmyer, Reticulated nanoporous polymers by controlled polymerization-induced microphase separation. *Science* **336**, 1422–1425 (2012).
19. H. Sai, K. W. Tan, K. Hur, E. Asenath-Smith, R. Hovden, Y. Jiang, M. Riccio, D. A. Muller, V. Elser, L. A. Estroff, S. M. Gruner, U. Wiesner, Hierarchical porous polymer scaffolds from block copolymers. *Science* **341**, 530–534 (2013).
20. K. W. Tan, B. Jung, J. G. Werner, E. R. Rhoades, M. O. Thompson, U. Wiesner, Transient laser heating induced hierarchical porous structures from block copolymer–directed self-assembly. *Science* **349**, 54–58 (2015).
21. H. Yu, X. Qiu, S. P. Nunes, K.-V. Peinemann, Biomimetic block copolymer particles with gated nanopores and ultrahigh protein sorption capacity. *Nat. Commun.* **5**, 4110 (2014).
22. S. P. Nunes, A. R. Behzad, B. Hooghan, R. Sougrat, M. Karunakaran, N. Pradeep, U. Vainio, K.-V. Peinemann, Switchable pH-responsive polymeric membranes prepared via block copolymer micelle assembly. *ACS Nano* **5**, 3516–3522 (2011).
23. W. A. Phillip, R. M. Dorin, J. Werner, E. M. V. Hoek, U. Wiesner, M. Elimelech, Tuning structure and properties of graded triblock terpolymer-based mesoporous and hybrid films. *Nano Lett.* **11**, 2892–2900 (2011).
24. H. Yu, X. Qui, A. R. Behzad, V. Musteata, D.-M. Smilgies, S. P. Nunes, K.-V. Peinemann, Asymmetric block copolymer membranes with ultrahigh porosity and hierarchical pore structure by plain solvent evaporation. *Chem. Commun.* **52**, 12064–12067 (2016).
25. A. Abbott, Cell culture: Biology's new dimension. *Nature* **424**, 870–872 (2003).
26. M. S. Silverstein, PolyHIPEs: Recent advances in emulsion-templated porous polymers. *Prog. Polym. Sci.* **39**, 199–234 (2014).
27. K. H. Wong, T. P. Davis, C. Barner-Kowollik, M. H. Stenzel, Honeycomb structured porous films from amphiphilic block copolymers prepared *via* RAFT polymerization. *Polymer* **48**, 4950–4965 (2007).
28. N. L. Le, S. P. Nunes, Materials and membrane technologies for water and energy sustainability. *Sustain. Mater. Technol.* **7**, 1–28 (2016).
29. A. Harada, R. Kobayashi, Y. Takashima, A. Hashidzume, H. Yamaguchi, Macroscopic self-assembly through molecular recognition. *Nat. Chem.* **3**, 34–37 (2011).
30. C. M. Hansen, *Hansen Solubility Parameters: A User's Handbook, Second Edition* (CRC Press, 2007).
31. S. P. Nunes, B. A. Wolf, H. E. Jeberien, On the cooccurrence of demixing and thermoreversible gelation of polymer solutions. 2. Thermodynamic background. *Macromolecules* **20**, 1948–1951 (1987).
32. P. Ball, *Shapes: Nature's Patterns: A Tapestry in Three Parts* (OUP Oxford, 2009).
33. R. Takekoh, T. P. Russell, Multi-length scale porous polymers. *Adv. Funct. Mater.* **24**, 1483–1489 (2014).
34. S. J. Kim, G. Chase, S. C. Jana, The role of mesopores in achieving high efficiency airborne nanoparticle filtration using aerogel monoliths. *Sep. Purif. Technol.* **166**, 48–54 (2016).
35. J. L. Weidman, R. A. Mulvenna, B. W. Boudouris, W. A. Phillip, Nanoporous block polymer thin films functionalized with bio-inspired ligands for the efficient capture of heavy metal ions from water. *ACS Appl. Mater. Interfaces* **9**, 19152–19160 (2017).
36. J. L. Weidman, R. A. Mulvenna, B. W. Boudouris, W. A. Phillip, Unusually stable hysteresis in the pH-response of poly(acrylic acid) brushes confined within nanoporous block polymer thin films. *J. Am. Chem. Soc.* **138**, 7030–7039 (2016).
37. X. Pang, Y. He, J. Jung, Z. Lin, 1D nanocrystals with precisely controlled dimensions, compositions, and architectures. *Science* **353**, 1268–1272 (2016).
38. H.-D. Yu, Z.-Y. Zhang, K. Y. Win, J. Chan, S. H. Teoh, M.-Y. Han, Bioinspired fabrication of 3D hierarchical porous nanomicrostructures of calcium carbonate for bone regeneration. *Chem. Commun.* **46**, 6578–6580 (2010).
39. A. S. Finnemore, M. R. J. Scherer, R. Langford, S. Mahajan, S. Ludwigs, F. C. Meldrum, U. Steiner, Nanostructured calcite single crystals with gyroid morphologies. *Adv. Mater.* **21**, 3928–3932 (2009).
40. J. Ilavsky, P. R. Jemian, *Irena*: Tool suite for modeling and analysis of small-angle scattering. *J. Appl. Cryst.* **42**, 347–353 (2009).

Acknowledgments: We thank LNLS (Brazil) for access at the SAXS1 beamline, particularly F. Meneau and T. A. Kakile for their help during measurements, T. M. D'Alvise for helpful discussions on the procedure for growing $CaCO_3$ crystals, P. N. Chitamb for the permeation measurement, and J. A. Palacio for help with the pore size statistics. **Funding:** This research was supported by the King Abdullah University of Science and Technology. **Author contributions:** S.C. designed the study, prepared all structures, and characterized the structures by SEM and spectroscopy. V.-E.M. performed SAXS experiments. R.S. performed the TEM imaging. A.R.B. performed serial block face SEM imaging. S.C. and S.P.N. proposed the formation mechanism and wrote the manuscript. **Competing interests:** The authors declare that they have no competing interests. **Data and materials availability:** All data needed to evaluate the conclusions in the paper are present in the paper and/or the Supplementary Materials. Additional data related to this paper may be requested from the authors.

Submitted 21 January 2018
Accepted 26 March 2018
Published 11 May 2018
10.1126/sciadv.aat0713

Citation: S. Chisca, V.-E. Musteata, R. Sougrat, A. R. Behzad, S. P. Nunes, Artificial 3D hierarchical and isotropic porous polymeric materials. *Sci. Adv.* **4**, eaat0713 (2018).